Interactive Effects of HRV and P-QRS-T on the Power Density Spectra of ECG Signals

Ting Xiang, Nan Ji, David A. Clifton, *Member, IEEE*, Lei Lu, and Yuan-Ting Zhang, *Fellow, IEEE*

Abstract—Different from the traditional methods of assessing the cardiac activities through heart rhythm statistics or P-QRS-T complexes separately, this study demonstrates their interactive effects on the power density spectrum (PDS) of ECG signal with applications for the diagnosis of ST-segment elevation myocardial infarction (STEMI) diseases. Firstly, a mathematical model of the PDS of ECG signal with a random pacing pulse train (PPT) mimicking S-A node firings was derived. Secondly, an experimental PDS analysis was performed on clinical ECG signals from 49 STEMI patients and 42 healthy subjects in PTB Diagnostic Database. It was found that besides the interactive effects which are consistent between theoretical and experimental results, the ECG PDSs of STEMI patients exhibited consistently significant power shift towards lower frequency range in ST-elevated leads in comparison with those of reference leads and leads of health subjects with the highest median frequency shift ratios at $51.39 \pm 12.94\%$ found in anterior MI. Thirdly, the results of ECG simulation with systematic changes in PPT firing statistics over various lengths of ECG data ranging from 10 s to 60 mins revealed that the mean and median frequency parameters were less affected by the heart rhythm statistics and the data length but more depended on the alterations of P-QRS-T complexes, which were further confirmed on 33 more STEMI patients in European ST-T Database, demonstrating that the frequency indexes could be potentially used as alternative indicators for STEMI diagnosis even with ultra-short-term ECG recordings suitable for wearable and mobile health applications in living-free environments.

Ting Xiang and Nan Ji are with the Department of Biomedical Engineering, City University of Hong Kong, Hong Kong SAR, China (e-mail: txiang@cityu.edu.hk; nanji3-c@my.cityu.edu.hk).

David A. Clifton is with the Department of Engineering Science, University of Oxford, OX1 2JD Oxford, U.K., and also with the Oxford-Suzhou Centre for Advanced Research, Suzhou, China (e-mail: david.clifton@eng.ox.ac.uk).

Lei Lu is with the Department of Engineering Science, University of Oxford, OX1 2JD Oxford, U.K. (e-mail: lei.lu@eng.ox.ac.uk).

Yuan-Ting Zhang is with the Hong Kong Center for Cerebro-cardiovascular Health Engineering (COCHE), Hong Kong Science and Technology Park, Hong Kong, and also with the Department of Biomedical Engineering at City University of Hong Kong, Hong Kong SAR, China (e-mail: yt.zhang@cityu.edu.hk, ytzhang@hkcoche.org).

Digital Object Identifier 10.1109/JBHI.2021.3100425

Index Terms—ECG, Frequency parameters, power density spectrum, STEMI, myocardial infarction.

INTRODUCTION

THE ELECTROCARDIOGRAM (ECG) record changes in the electrical activity generated by the heart during each cardiac cycle from the body surface, which has been widely used for diagnosing and monitoring abnormal heart conditions [1]. Heart rate variability (HRV) refers to the fluctuation between the intervals of consecutive heart beats (R-R intervals, RRIs), which is a powerful quantitative index to assess cardiac dynamics and the state of the Autonomic Nervous System (ANS) responsible for regulating cardiac rhythm and cardiac activity. It has been shown that the HRV analysis provides a reliable reflection of the balance between the Sympathetic Nervous Systems (SNS) and Parasympathetic Nervous Systems (PNS), which is a valuable non-invasive parameter for assessing the function of the ANS and the status of various heart diseases [2]. Numerous studies have suggested that decreased HRV is an adverse prognostic factor for many cardiovascular diseases [3], [4]. Depressed HRV, which is empirically defined as SDNN (standard deviation of normal RRIs) <100 ms and HRV triangular index (the integral of the density distribution divided by the maximum of the density distribution) <20, is a powerful predictor of risk in patients following acute myocardial infarction (MI). Several studies have found that lower HRV is associated with a higher risk of mortality in survivors of an acute MI. Post-MI patients whose SDNN less than 70 ms on 24-hours ECG recording, were found to have 4 times more chance of mortality compared to those who have SDNN above 70 ms. Hence, HRV is widely used as a prognostic factor for MI risk stratification and management [5], [6], [7]. Due to the need for monitoring individual's health and well-being status, the interests in ultra-short-term HRV analysis with its applications in wearable devices and mobile health technology are significantly increasing recently [8], [9], [10].

The main methods for HRV analysis include time domain analysis, frequency domain analysis and nonlinear analysis. Time domain methods for analyzing ECG recordings focus on statistical analysis, including mean heart rate, standard deviation of normal RRIs (SDNN), and other variables derived from RRIs such as the standard deviation of differences between adjacent normal RRIs (SDSD), the root mean square of successive difference of intervals (RMSSD) and the number of adjacent interval pairs that differ more than 50 ms (NN50) [3], [4]. In frequency domain, the spectral components of HRV calculated from RRI series of ECG recordings include 0.0033-0.04 Hz for very low

frequency (VLF) component, 0.04-0.15 Hz for low frequency (LF) component, and 0.15-0.4 Hz for high frequency (HF) component. Studies have shown that LF reflects the regulation of SNS and PNS while HF only reflects the regulation of the PNS and the LF/HF ratio reflects the balance of the ANS [3], [4], [5]. For nonlinear analysis, a specific subtype of nonlinear dynamics, chaos theory and fractals [11], [12] has been applied to HRV study. The nonlinear analysis method is mostly at theoretical stage and needs further studies of clinical applications [7].

Myocardial infarction (MI) is a leading component of the cardiovascular diseases. ST-segment elevation myocardial infarction (STEMI) is a life-threatening, time-sensitive emergency condition which will cause rapid and irreversible damage to cardiac muscle. So STEMI patients must be diagnosed and treated promptly [13], [14]. The abnormal alterations in the cardiac electrical activity are commonly used to diagnose and evaluate the STEMI development reflected by the P-QRS-T complexes changes in the 12-lead ECG, which is still the most easily available and noninvasive procedure for the early diagnosis of MI [15]. In the clinical guideline, ST-segment elevation showed in the P-QRS-T complexes is considered STEMI when the elevation level is higher than the clinical scopes for different groups [14]. Additionally, different ECG leads showing significant ST-segment elevations are indicative of the ischemic area, which can be used to classify the types of STEMI, such as anterior MI, inferior MI and lateral MI, and their combinations such as antero-septal MI and antero-laterl MI. The signs of ST-segment elevation can be seen in leads II, III and avF for inferior MI, leads V3 and V4 for anterior MI, leads V1 to V4 for anterior-septal MI, leads V3 to V6 for antero-lateral MI, and leads I and avL for lateral MI [15], [16], [17]. Hence, previous studies have proposed various methods for MI detection and localization. Most recently, some approaches like optimal biorthogonal filter bank [18], sonification method [19], Fourier-Bessel series expansion-based empirical wavelet transform (FBSE-EWT) [20] and automatic algorithm based on staked sparse autoencoder and bagged decision tree [21], have been proposed to improve the accuracy of MI detection and localization.

It is known that the ECG signal can be regarded as a composite signal with multiple frequency components produced by various physiological processes in addition to the pacing patterns generated from the S-A node. Therefore, any abnormalities in these physiological processes may lead to variations in the power distribution between constituent frequencies [22]. However, most of studies so far simply either calculate the statistical parameters and/or the spectra of RRIs to study cardiovascular activities, or concentrate only on the P-QRS-T complexes analysis, rather than the analysis of the complete ECG signals with both heart beat intervals and the waveforms, which reflect the wholistic heart neural-physiological-electrical activities.

It was hypothesized that the subtle changes in the P-QRS-T complexes during each cardiac cycle would affect the changes in power at each frequency component of ECG signal [22]. The results intuitively showed that the ECG spectra of healthy subjects had less power distribution in the high frequency range, and less variability than that from patients with arrhythmia. For normal subjects, the power distribution was generally concentrated around 1 Hz with low variability in the ECG spectrum, while the power range extended to 4-5 Hz with higher variability for patients with arrhythmia [22]. Although the method has been examined on the whole ECG signal, it lacked a theoretical basis to explain the variations of ECG power spectrum and failed to quantify some phenomena.

In this work, a mathematical model for ECG signal generation was proposed with the P-QRS-T complexes as the impulse response of a linear time-invariant system and a pacing pulse train (PPT) with random R-R intervals (RRIs) mimicking the S-A node fittings as the input to the system [1]. Based on the model we derived equations showing the interactive effects of heart rate (HR), its variability and P-QRS-T complexes on the PDS of ECG signal. Then, the PDS analysis of clinical ECG recordings of STEMI patients from existing databases was carried out to verify the theoretical results and to study possible new indicators for the diagnosis of STEMI diseases. Finally, the ECG simulation with a given P-QRS-T waveform and various values of HR and HRV in the physiological range was performed to investigate their effects on the new frequency indicators. Furthermore, the new indicators were studied on different segment lengths of clinical ECG recordings with ST-segment elevation to investigate the effects of the length of ECG recording and the reliability of the new indicators in ultra-short-term ECG recordings.

II. METHODS

A. A Mathematical Model and PDS of ECG Signals

ECG activity, which reflects a continuous process of depolarization and repolarization in the myocardial conduction system, normally begins in the S-A node and successively excites atrium and ventricle, causing the heart to contract and pump blood to the lungs and the whole body [1].

In general, neural electrical impulses at the S-A node do not occur periodically with perfect regularity. Instead, they exhibit random variations around the mean heart rate/firing rate. Thus, as the firing of S-A node is affected by the ANS input, the RRIs extracted from the ECG signal exhibit stochastic characteristics [23], [24]. To simulate the physiological generation of ECG signal, a linear time-invariant system model was proposed as shown in Fig. 1. The input signal $p(t)$ to the system represents the PPT, simulating the electrical activities originated at the S-A node, which is a sequence of pulses with discrete random occurrences in continuous time [1], [25] and, as such it was approximated as a renewal random point process with known activation statistics [26], [27], [28]. The impulse response $e(t)$ of system represents the P-QRS-T complex of ECG signal. Although there are many different structures of linear time invariant filters available to describe P-QRS-T waveforms [29], the P-QRS-T complex in the model was extracted directly from the clinical ECG signals with several motivations including 1) to develop new indicators of STEMI diseases using ultra-short-term segment of real-world data for possible wearable and mobile health applications; 2) to avoid possible errors that might be caused by a mathematical model of the P-QRS-T complex and its parameter selections in the estimation of the proposed new indicators/indexes; and 3) to
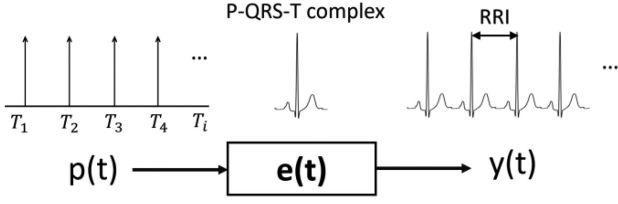
Fig. 1. A generation model of ECG signal.

study the interactive effects of RRI statistics of PPT mimicking the signal generation from S-A node with the real P-QRS-T complex of clinical recordings on the proposed new indicators. The output $y(t)$ of the model represents theoretical ECG signal which is determined by the pacing pulse train from S-A node and the P-QRS-T complex reflecting heart contraction dynamics.

The PPT can be approximate to a sequence of impulses described as:

$$p\left(t\right) = \sum_{i=-\infty}^{\infty} \delta\left(t - T_i\right) \quad (1)$$

where a random variable T_i represents the on-set time of each ECG cycle. The instantaneous pacing/heart rate, λ_i, can be described as:

$$\lambda_i = \frac{1}{T_i - T_{i-1}} \quad (2)$$

The PDS, $\Phi_{pp}(f)$ of the model output $y(t)$ representing ECG signal is expressed as:

$$\Phi_{yy}\left(f\right) = \Phi_{pp}\left(f\right) \left|E\left(f\right)\right|^2 \quad (3)$$

where $\Phi_{pp}(f)$ is the PDS of the PPT and $E(f)$ is the Fourier transform of $e(t)$. The PDS of ECG signal in (3) is the product of $|E(f)|^2$, the energy spectrum of the P-QRS-T complex associated with the cardiac contraction dynamics, and $\Phi_{pp}(f)$, the PDS of the pacing pulse train reflecting the S-A node firing patterns. The R-R intervals between successive impulses can be approximated as a sequence of independently distributed random variables with a probability density function (PDF), $f_x(x)$ [30]. For a renewal random point process, the PDS of the pacing pulse train can be described as [30], [31], [32], [33],

$$\Phi_{pp}\left(f\right) = \lambda\left(1 + \frac{F_x\left(f\right)}{1 - F_x\left(f\right)} + \frac{F_x^*\left(f\right)}{1 - F_x^*\left(f\right)}\right), f \neq 0 \quad (4)$$

where $F_x(f)$ represents the Fourier transform of the PDF $f_x(x)$ of RRIs, $F_x^*(f)$ is the complex conjugate of $F_x(f)$, and λ is the mean pacing/heart rate of the ECG signal in pulse per second (pps). This formula form was applied in distributed random electrical neuromuscular stimulation and the spectral analysis of electromagnetic signals previously [27], [28]. For a given PDF, the PPT, combining (3) and (4) yields the PDS of ECG signal,

$$\Phi_{yy}\left(f\right)$$
$$= \lambda\left(1 + \frac{F_x\left(f\right)}{1 - F_x\left(f\right)} + \frac{F_x^*\left(f\right)}{1 - F_x^*\left(f\right)}\right) \left|E\left(f\right)\right|^2, f \neq 0 \quad (5)$$

In this study, RRIs of the ECG signal are assumed to be with a Gaussian PDF, $f_x(x)$. With this assumption, the PDS of ECG signal can be obtained by (6). The detailed deviation of (6) is given in the Appendix I,

$$\Phi_{yy}\left(f\right) = \lambda \frac{\sinh\left[2(\pi f \sigma_x)^2\right]}{\cosh\left[2(\pi f \sigma_x)^2\right] - \cos\left(\frac{2\pi f}{\lambda}\right)} \left|E\left(f\right)\right|^2, f \neq 0 \quad (6)$$

where σ_x is the standard deviation of the RRIs, HRV and c is the variation coefficient defined by $c = \sigma_x \lambda$ representing the normalized HRV.

B. Experimental ECG Data Analysis

The raw ECG datasets analyzed in this study were obtained from PTB Diagnostic Database (PTBDB) and European ST-T Database (EDB) in 'Physionet' [34]. Each ECG recording in PTBDB includes the conventional 12 leads (I, II, III, avR, avL, avF, V1, V2, V3, V4, V5, V6) together with 3 Frank leads (Vx, Vy, Vz). Each subject in EDB was diagnosed or suspected as myocardial ischemia, the ECG recordings of which are two hours in duration and contain two leads. The standard limb leads (I, II, III) and chest leads recordings (V1, V2, V3, V4, V5, V6) of 60 s in PTBDB and ECG recordings of 60 mins in EDB were analyzed in our study.

Previous studies suggested that some factors such as recording method and motion artifact may have greater impact on ultra-short-term measurements compared with long-term recordings. Especially, the bias introduced by even a single artifact will easily influence the analysis results, indicating that it is necessary to carefully remove artifacts and select artifact-free epoch when using ultra-short-term recordings [8], [35]. To test the normality of RRI data with ultra-short segment length, we used 42 ECG recordings of 60 s from healthy subjects and 49 ECG recordings from STEMI patients in PTBDB after excluding raw ECG recordings with artifactual interbeat intervals by visual inspection. The Kolmogorov-Smirnov (KS) Test [36] was conducted by Matlab to study the distribution of RRIs with 5% critical values. The RRIs distribution can be regarded as Gaussian distribution if a p-value is greater than 0.05.

In order to evaluate and quantify the power distributions showed in the PDSs of ECG signals with different HRs, HRVs and P-QRS-T complexes, the mean frequency, MNF, and the median frequency, MDF of PDSs were calculated from 0.05 Hz to 100 Hz, which contained most of the useful information about the ECG signals in frequency domain [37].

In our study, the leads without ST-segment elevation in STEMI patients were regarded as reference leads. The frequency shift ratio of MNF or MDF was defined as the quotient of the difference in the frequency parameters between the reference lead and the ST-elevated lead divided by the frequency parameter of the reference lead.

The criteria of excluding severe artifacts and baseline wander were established to obtain relatively stable and high-quality ECG signals. 98 ECG datasets of 60 s from 49 STEMI patients and 210 ECG datasets of 60 s from 42 healthy subjects in PTBDB were included for PDS analysis. For STEMI patients, the MNF

and MDF of the reference leads and ST-elevated leads including lead I, V3 (anterior MI, n = 12), leads I, V2 (antero-septal MI, n = 21) and leads V5, III (inferior MI, n = 16) were calculated. Correspondingly, the MNF and MDF of the leads I, V5 and leads III, V2, V3 in 42 healthy subjects were also calculated for comparison with reference leads (leads I, V5) and ST-elevated leads (leads III, V2, V3) of STEMI patients. 33 ECG datasets with ST-segment elevation of 60 mins from 33 MI patients in EDB were selected to calculate the HRV, MNF and MDF over different segment lengths ranging from the ultra-short-term of 10 s to 60 mins.

Numerical variables were expressed as Mean ± SD. Comparisons for numerical variables were made using Student's t-test and the value was considered significant when $p < 0.01$.

C. Simulation of ECG Signals

The ECG signals were simulated based on a linear time-invariant filtering system model. The input signal representing electrical propagating activation originated at the S-A node was simulated using a random point process with Gaussian distributed PPTs assigned with practical values within the ranges studied in clinical ECG signals, and the impulse responses representing the P-QRS-T complex associated with the cardiac contraction dynamics. The simulated ECG were generated by convoluting the pacing pulse train with P-QRS-T complex, which was randomly extracted from a cycle of the clinical ECG recordings in terms of the typical morphology described in [1], [14] by eyeballing.

The ECG simulation model was implemented in Matlab. The PDS and frequency parameters were calculated from simulated ECG with the time length of 60 s. The consistency between the frequency parameters of simulated ECGs and clinical ECGs was evaluated in terms of the normalized difference. The interactive effects of PPT statistics and P-QRS-T complex on the PDSs and frequency parameters were analyzed using simulated ECGs with various values of HRs, HRVs, and a same P-QRS-T complex extracted from a STEMI patient.

Furthermore, mean absolute percentage error (MAPE) between the frequency parameters calculated from the simulated ECG PDSs of different lengths and those of the theoretical PDSs were used to evaluate the influence of the signal segment length on the accuracy of MNF and MDF.

III. RESULTS AND DISCUSSIONS

A. The Distribution of RRIs of Clinical ECG Signals

Results of the KS test showed that most of the ECG recordings from healthy subjects and MI patients of 60 s had p-value greater than 0.05. The test results indicated that the RRIs of the majority of ultra-short-term clinical ECG signals can be approximated as Gaussian distribution.

B. Power Spectral Analysis of Clinical ECG Signals

For the purpose of comparing the spectra of ECG recordings with different mean heart rate, λ, standard deviation of the RRIs, HRV, σ_x, and coefficient of the RRIs, normalized HRV, c, the
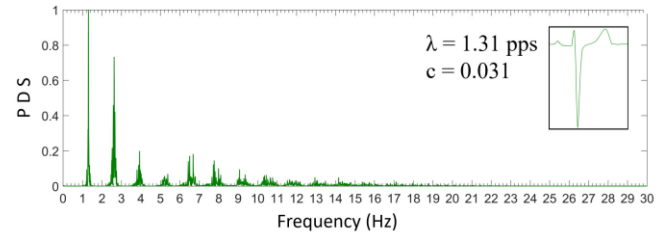

Fig. 2.   The PDS of a typical healthy ECG signal (s0452).
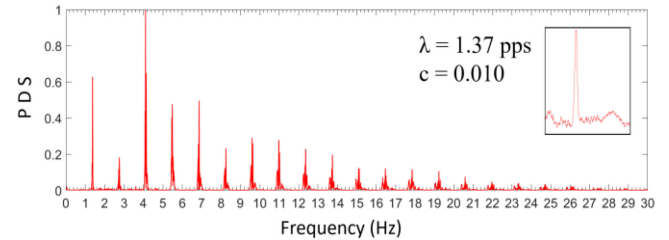

Fig. 3.   The PDS of lead I (standard limb lead) ECG signal from a STEMI patient (s0020).

amplitudes of the ECG PDS were normalized according to their maximum values. The PDSs of ECG signals were plotted in the range of 0.05-30 Hz.

The features of theoretical PDS of ECG signal with the Gaussian distributed RRIs, supported by experimental results of clinical ECG signals, are summarized as follows [27]:

1) The ECG PDS has normally peaks at harmonics of the mean pacing/heart rate for the RRIs with Gaussian PDF $f_x(x)$. This observation can be deduced from (6). The spectral peaks of the ECG PDS are generated by the cosine component in (6) with $f = k\lambda$, (k = 1, 2, 3 …). Besides, the frequency corresponding to the first peak is equal to the λ. This observation from the mathematical model can be seen in the experimental PDS of ECG signal as illustrated in Fig. 2 showing the PDS from a normal subject with values of λ = 1.31 pps and c = 0.031.

2) The magnitudes and the numbers of the peaks in the ECG PDS rely on the normalized HRV, c. This phenomenon can be explained by substituting $f = k\lambda$ into (6) for the Gaussian intervals. Equation (6) becomes,

$$\Phi_{yy}(f, c) = \lambda \frac{\sinh\left[2(\pi k c)^2\right]}{\cosh\left[2(\pi k c)^2\right] - 1} |E(f)|^2, f \neq 0 \quad (7)$$

The magnitudes of most peaks in ECG PDS become large when the normalized HRV, c is small. This trend can be seen in the experimental result in Fig. 3, where the magnitudes of most peaks are higher with a smaller c in comparison with that in Fig. 2. The number of the peaks in the PDS is also influenced by the value of c, which can be verified by (7) and illustrated in Figs. 2 and 3.

3) The PDS of ECG signal depends not only on the c as seen above but also on the spectrum of P-QRS-T complex, $E(f)$ as expected. Substituting (6) for $\Phi_{pp}(f)$ with a

| Anterior MI	Mean frequency			Median frequency		
(n=12)	Lead I (Hz)	Lead V3 (Hz)	Shift ratio	Lead I (Hz)	Lead V3 (Hz)	Shift ratio
1	10.39	6.15	40.81%	9.22	4.02	56.40%
2	15.23	5.82	61.79%	14.13	3.40	75.94%
3	9.00	6.82	24.22%	7.58	4.69	38.13%
4	13.16	6.03	54.18%	11.93	3.92	67.14%
5	14.22	8.08	43.18%	14.15	7.11	49.75%
6	8.54	6.71	27.75%	7.22	5.4	25.21%
7	9.97	5.55	44.33%	9.36	3.93	58.01%
8	10.45	5.76	44.88%	8.29	3.68	55.61%
9	11.00	8.16	25.82%	9.35	4.70	49.73%
10	10.63	7.17	32.55%	9.58	4.15	56.68%
11	13.11	8.42	35.77%	12.38	7.08	42.81%
12	10.40	7.91	23.94%	8.73	5.13	41.24%
Mean±SD	11.34±2.01	6.88±1.00	38.27±11.64%	10.16±2.29	4.77±1.18	51.39±12.94%
p-value	<0.0001			<0.0001		
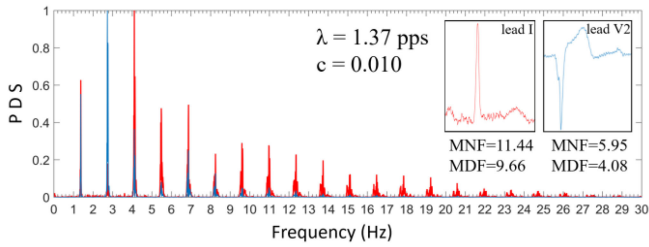
Fig. 4. The comparison of the PDS of lead I (standard limb lead) ECG signal showed in Fig. 3 (red) and the PDS of lead V2 (chest lead) ECG signal (blue) from the same MI patient.

Gaussian distributed RRIs, let $\sigma_x = \sigma$, the PDS in (6) can be written as,

$$\Phi_{yy}(f) = \lambda \frac{\sinh\left[2(\pi f \sigma)^2\right]}{\cosh\left[2(\pi f \sigma)^2\right] - 1} |E(f)|^2, f \neq 0 \quad (8)$$

Equation (8) illustrates that the PDS envelope of ECG signal is controlled by the spectrum, $E(f)$ while the detailed changes in the PDS are associated with the RRIs statistics under various conditions. In Fig. 4, the ECG PDS of lead I (standard limb lead) is compared with the lead V2 (chest lead) showing ST-segment elevation in the same STEMI person, which have different P-QRS-T complexes but the same values for λ and c. It can be seen that the amplitudes of spectral peaks distributed in low frequency range of lead V2 are higher than those of lead I as reference lead in the same MI patients. For the lead V2, the main power distribution generally shifts towards the low frequency range below 5-8 Hz while for the lead I, the power range extends to 8-15 Hz with higher variability in the spectrum. The spectral differences between the lead I and lead V2 are resulted from the different P-QRS-T complexes in the time domain.

As described above, the ECG is a compound signal with many frequency components generated during heart contraction dynamics in addition to the PPT frequency components which

associated with distinct neural-physiological processes. Any abnormality in the processes and heart contraction dynamics could lead to variations in the PDS [22], [38], suggesting the importance and the necessity to extract frequency domain indicators for the diagnosis of cardiovascular diseases. In Fig. 4, the MNF and MDF of the PDSs were calculated in lead I and lead V2 respectively, which were lower in lead V2 (MNF = 5.95 Hz, MDF = 4.08 Hz) than in lead I (MNF = 11.44 Hz, MDF = 9.66 Hz), indicating MNF and MDF maybe possible indicators to diagnose STEMI through evaluating and quantifying the power shift in the PDSs caused by the changes of P-QRS-T complexes in different leads.

C. Statistical Analysis of Clinical ECG Signal

The results of MNF and MDF of reference leads, ST-elevated leads and their shift ratios for anterior MI (n = 12), antero-septal MI (n = 21), and inferior MI (n = 16) were showed in Tables I, II and III respectively.

It can be seen from Tables I, II and III that all the values of MNF and MDF were lower in ST-elevated leads compared with the reference leads for STEMI patients. For anterior MI, MNF and MDF in lead V3 were statistically significant lower than in lead I (6.88 ± 1.00 Hz vs 11.34 ± 2.01 Hz, p < 0.0001; 4.77 ± 1.18 Hz vs 10.16 ± 2.29 Hz, p < 0.0001). Similarly, MNF and MDF in ST-elevated leads were statistically significant lower than in reference leads for antero-septal MI (6.64 ± 1.12 Hz vs 10.67 ± 1.94 Hz, p < 0.0001; 4.70 ± 1.05 Hz vs 9.14 ± 2.02 Hz, p < 0.0001) and for inferior MI (7.83 ±1.54 Hz vs 12.48 ± 1.96 Hz, p < 0.0001; 5.42 ± 1.45 Hz vs 11.38 ± 2.26 Hz, p < 0.0001). The shift ratios of MNF and MDF were 38.27 ± 11.64% and 51.39 ± 12.94% in anterior MI, 37.86 ± 10.83% and 47.41 ± 10.80% in antero-septal MI, 36.06 ± 14.93% and 50.72 ± 15.56% in inferior MI.

In addition to the statistical analysis on MNF, MDF and their shift ratios of 3 types of STEMI separately, data from these 3 types of STEMI were combined for subsequent analyses with comparison of healthy subjects. The box plots in Fig. 5 showed the full distribution of the frequency parameters and their shift

TABLE II
MEAN FREQUENCY AND MEDIAN FREQUENCY OF ANTERO-SEPTAL MI

Antero-septal MI (n=21)	Mean frequency			Median frequency		
	Lead I (Hz)	Lead V2 (Hz)	Shift ratio	Lead I (Hz)	Lead V2 (Hz)	Shift ratio
1	11.44	5.95	47.99%	9.66	4.08	57.76%
2	12.59	8.86	29.63%	10.04	7.14	28.88%
3	13.25	5.78	56.38%	11.87	4.38	63.10%
4	10.07	5.91	47.67%	8.79	4.82	45.16%
5	11.15	6.09	45.38%	8.33	4.86	41.66%
6	14.47	6.42	55.63%	13.29	4.95	62.75%
7	8.96	5.40	39.73%	6.66	3.97	40.39%
8	10.89	6.59	39.49%	9.91	4.11	58.53%
9	11.76	7.63	35.12%	9.92	6.17	37.80%
10	11.88	9.07	23.65%	10.40	7.13	31.44%
11	10.47	6.93	33.81%	9.44	4.80	49.15%
12	9.36	7.40	20.94%	8.59	5.32	38.07%
13	6.26	4.25	32.11%	5.48	2.78	49.27%
14	8.11	5.94	26.76%	6.73	4.10	39.08%
15	11.18	7.33	34.44%	8.61	4.65	45.99%
16	10.20	6.02	40.98%	8.60	4.25	50.58%
17	8.70	6.62	23.91%	7.39	3.58	51.56%
18	13.76	5.38	60.90%	13.83	3.88	71.95%
19	8.80	5.93	32.61%	7.41	3.72	49.80%
20	9.38	6.08	35.18%	7.88	5.13	34.90%
21	11.42	7.68	32.75%	9.18	4.79	47.82%
Mean±SD	10.67±1.94	6.64±1.12	37.86±10.83%	9.14±2.02	4.70±1.05	47.41±10.80%
p-value	<0.0001			<0.0001		

TABLE III
MEAN FREQUENCY AND MEDIAN FREQUENCY OF INFERIOR MI

Inferior MI (n=16)	Mean frequency			Median frequency		
	Lead V5 (Hz)	Lead III (Hz)	Shift ratio	Lead V5 (Hz)	Lead III (Hz)	Shift ratio
1	15.82	10.23	35.34%	14.93	9.03	39.52%
2	11.14	7.11	36.18%	10.58	4.41	58.32%
3	13.31	9.51	28.55%	11.58	6.28	45.77%
4	10.26	8.86	13.65%	8.69	6.17	29.00%
5	13.67	5.88	56.99%	12.58	3.81	69.71%
6	13.14	6.94	47.18%	12.60	4.73	62.46%
7	11.55	6.42	44.42%	10.54	4.88	53.70%
8	11.75	8.92	24.09%	10.68	4.93	53.84%
9	11.58	6.43	44.47%	9.97	3.85	61.38%
10	10.84	6.70	38.19%	9.36	4.05	56.73%
11	14.26	5.47	61.64%	13.50	4.07	69.85%
12	10.05	9.12	9.25%	8.53	6.88	19.34%
13	11.87	6.46	45.58%	10.70	4.48	58.13%
14	11.09	7.89	28.85%	9.53	6.69	29.80%
15	17.46	8.99	48.51%	17.24	5.10	70.42%
16	11.99	10.31	14.01%	11.03	7.33	33.54%
Mean±SD	12.48±1.96	7.83±1.54	36.06±14.93%	11.38±2.26	5.42±1.45	50.72±15.56%
p-value	<0.0001			<0.0001		

ratios between healthy subjects and 3 types of STEMI patients in our study. It can be seen in Fig 5(a), on average, the MNF of leads I, V5 (10.55 Hz) and leads III, V2, V3 (10.34 Hz) of healthy subjects and reference leads (11.43 Hz) of STEMI patients were distributed in higher ranges compared with ST-elevated leads (7.04 Hz). Similar results were noted for MDF, that the MDF distributed within a lower range in ST-elevated leads (4.95 Hz) compared with normal leads (8.83 Hz, 8.68 Hz) from healthy subjects and reference leads of STEMI patients (10.12 Hz). There were no significant differences between the MNF (p < 0.39) and MDF (p < 0.59) of leads I, V5 (corresponding to reference leads) and leads III, V2, V3 (corresponding to ST-elevated leads) of healthy subjects while the MNF and MDF (p < 0.0001) of ST-elevated leads were significantly lower than

in reference leads by the paired Student's t-test. The MNF shift ratios and the MDF shift ratios of STEMI patients were 37.37% and 49.47% respectively, showing consistent frequency shift towards the lower frequency range in the ST-elevated leads compared with those reference leads, while the shift ratios of MNF and MDF in healthy subjects presented lower shift ratios and even negative values. Besides, the statistical results showed that there were significant differences between the MNF, MDF based shift ratios of healthy subjects and those of STEMI patients (p < 0.0001). Thus, all the results strongly suggested that the feasibility of using MNF and MDF and their shift ratios calculated from the PDS of ultra-short-term ECG for the preliminary screening of STEMI and distinguish healthy people from STEMI patients.

TABLE IV
FREQUENCY PARAMETERS OF PDS OF ECG SIGNAL FROM PATIENTS WITH DIFFERENT TYPE OF STEMI

| Type	ECG lead	Mean Frequency (Hz)			Median Frequency (Hz)		
		Clinical Data	*Simulation*	*Normalized Difference*	*Clinical Data*	*Simulation*	*Normalized Difference*
Antero-septal MI	*Lead I*	8.96	8.8136	1.63%	6.66	6.5833	1.15%
	Lead V2	5.40	5.4418	0.77%	3.97	3.9583	0.29%
	Shift Ratio	39.73%	38.26%		40.39%	39.87%	
Anterior MI	*Lead I*	10.39	10.8007	3.95%	9.22	9.4833	2.86%
	Lead V3	6.15	6.148	0.03%	4.02	3.9833	0.91%
	Shift Ratio	40.81%	43.08%		56.40%	58.00%	
Inferior MI	*Lead V5*	10.84	10.9533	1.05%	9.36	9.4	0.43%
	Lead III	6.70	7.2659	8.45%	4.05	4.0833	0.82%
	Shift Ratio	38.19%	33.66%		56.73%	56.56%	
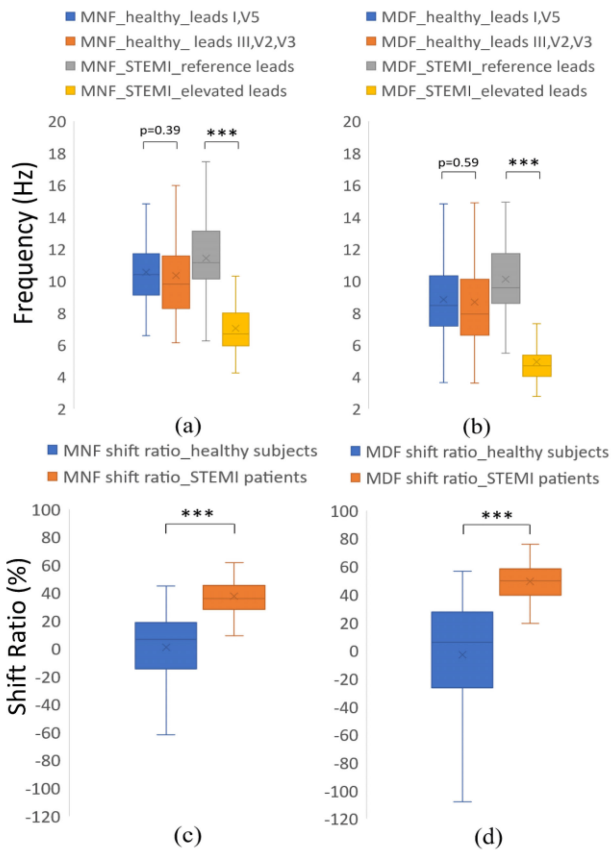
Fig. 5. Boxplots of (a) MNF and (b) MDF among leads I, V5 (corresponding to reference leads of STEMI patients), leads III, V2, V3 (corresponding to elevated leads of STEMI patients) in healthy subjects, reference leads and ST-elevated leads of three types of STEMI; (c) MNF shift ratio and (d) MDF shift ratio of healthy subjects and STEMI patients. The boxes display median, 25th, 75th percentiles (solid line), mean (cross), and the whiskers indicate the range of values excluding outliers. "∗∗∗" indicates statistical significance at p < 0.0001.

Fig. 6. Comparison of frequency parameters between PDSs of clinical ECG and simulated ECG over different segment lengths.

D. Results of ECG Simulation

The results of MNF and MDF of PDSs of clinical ECGs and simulation ECGs of 60 s and their normalized differences in three cases randomly selected from three types of STEMI in PTBDB were shown in Table IV. It was observed in Table IV that the normalized differences between clinical and simulation ECG in all three cases were within 9%. Additionally, the frequency parameters calculated from the PDSs of a longer clinical ECG
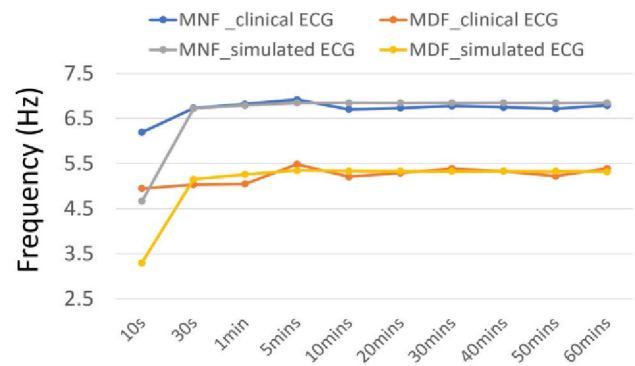
with ST-segment elevation randomly selected from EBD and the corresponding simulated STEMI ECG over different segment lengths ranging from 10 s to 60 mins were presented in Fig. 6. It can be seen that the normalized differences of MNF and MDF between clinical and simulated ECG calculated from different segments were within 5% when the lengths of ECG signals were longer than 30 s. The small errors confirmed that the proposed approach of using the extracted P-QRS-T complex as the response approximation of a linear time-invariant filtering system worked well in simulating clinical ECG in terms of its PDS. Additionally, the frequency parameters calculated from PDSs of simulated ECGs were in close agreement with those calculated from PDSs of clinical ECGs.

The plots of MNF as the function of PPT statistics were given in Figs. 7(a) and 7(c). It can be seen in Fig. 7(a) that the MNF increased slightly as the HR, λ increased from 0.7 to 1.7 Hz for the given different values of HRV, σ. Fig. 7(c) showed that for different values of λ, the MNF remained nearly constant in the studied range of σ. According to the definition of mean frequency, the larger λ leads the peaks of the PDS associated with HR to move towards higher frequency range, so accordingly the power distribution shifted to higher frequency range, which resulted in a higher MNF. Based on the observation that the magnitudes and the numbers of peaks in PDS depend on HRV, the small changes in σ contributed little effects on the PDS and thus, MNF basically remained steady with increasing values of σ.

In contrast, the apparently nonlinear relations between the MDF and PPT statistics can be seen in Figs. 7(b) and 7(d).
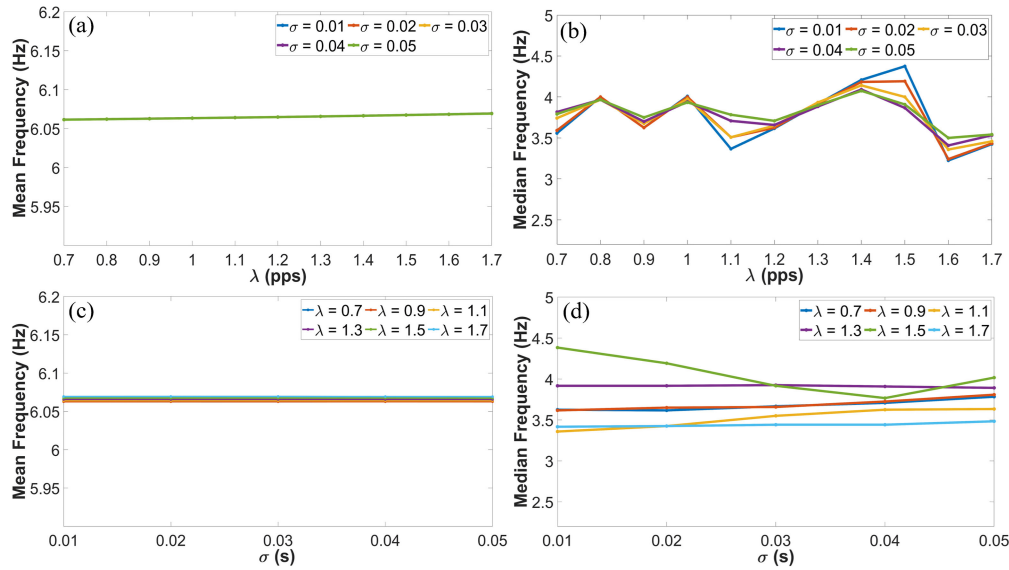
Fig. 7.   Frequency parameters of PDS. (a) Mean frequency and (b) Median frequency of the PDS as a function of λ for different values of σ. (c) Mean frequency and (d) Median frequency of the PDS as a function of σ for different values of λ.
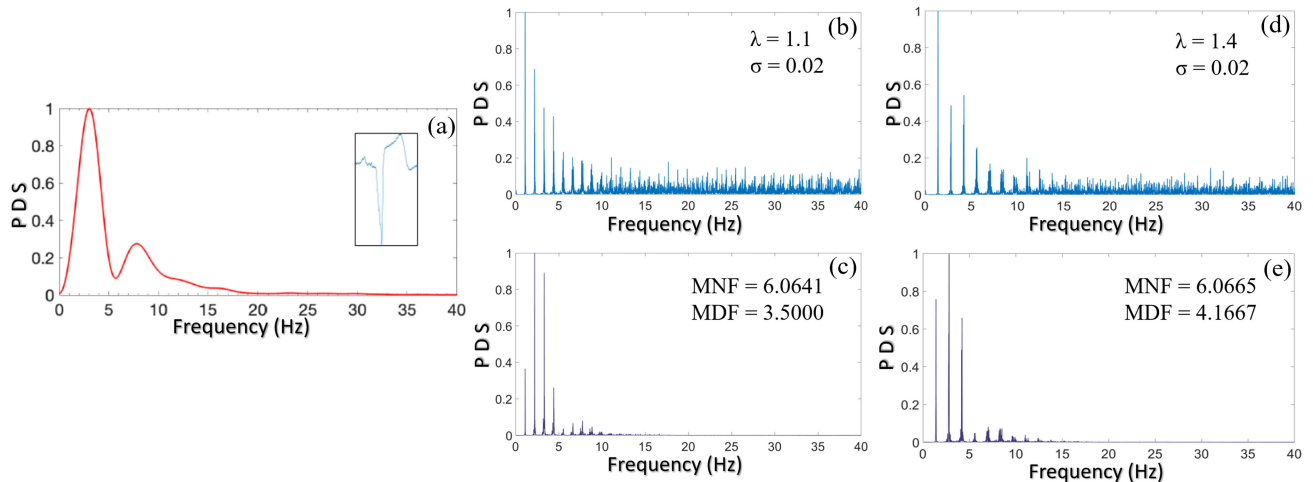

Fig. 8.   Effects of changes in λ on the PDS of the ECG signal for σ=0.02: (a) power spectrum of the P-QSR-T complex extracted from a STEMI patient; (b) (d) PDSs of simulated PPT with λ=1.1 and λ=1.4; and (c) (e) PDSs of the ECG signals from multiplying (a) by (b) and multiplying (a) by (d), respectively.

According to (3), the PDS of ECG signal was the multiplication of the PDS of the PPT, $\Phi_{pp}(f)$ and the spectrum of P-QRS-T complex, $|E(f)|^2$. Hence, the spectra in Fig. 8 were $|E(f)|^2$ of P-QRS-T complex extracted from a ST-elevated lead (Fig. 8(a)), the PDS $\Phi_{pp}(f)$ of PPT generated randomly with Gaussian distribution in 60 s (Figs. 8(b) and 8(d)) and their products $\Phi_{yy}(f)$, the PDS of simulated ECG (Figs. 8(c) and 8(e)). It was noted from Fig. 8 and corresponding equations that with the same power spectrum of P-QRS-T complex, the PDSs of PPT with different statistics leads to different distributions of the main peaks in ECG PDSs. Furthermore, MDF is theoretically governed by the central tendency [39], meaning that MDF is susceptible to the varying magnitudes and locations of the main

peaks in PDSs, which explains why the MDF moved up and down and out-of-order as the function of PPT statistics.

E. Effects of the Length of ECG Recording and Ultra-Short-Term HRV

The MAPE of the MNF and MDF between the PDS of simulated ECG and theoretical PDS for different values of σ within physiological range were calculated on each segment of 10 s, 30 s, 1 min, 5 mins, 10 mins, 20 mins, 30 mins, 40 mins, 50 mins and 60 mins, results of which were shown in Fig. 9. It can be seen that with increasing in the length of the ECG recording, the MAPEs of MNF, MDF deceased significantly
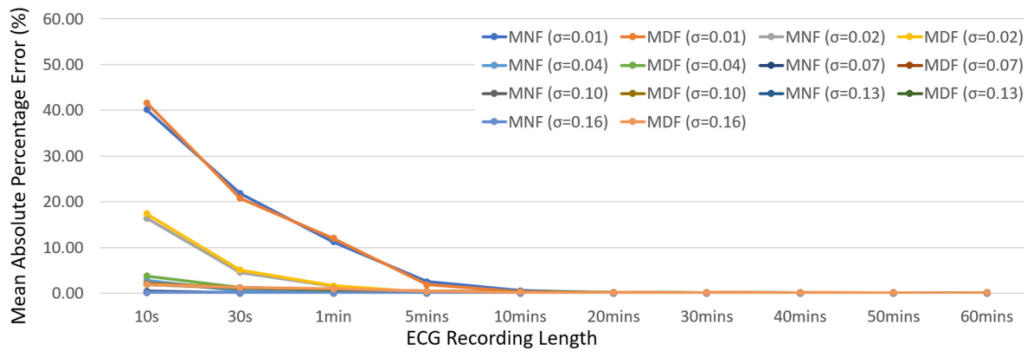
Fig. 9. The trend of the MAPE of MNF and MDF between the PDS of simulated ECG and theoretical PDS for different values of σ, HRV over different ECG lengths.

for all the values of σ and trended to approach zero when the length of the data segment was longer than 5 mins. It should be noted that for the ultra-short segment length of 1 min, the maximal MAPEs of MNF and MDF were 11.21% and 12.04% respectively when σ equaled to 0.01. The MAPEs of MNF and MDF decreased to 1.58% and 1.66% when σ equaled to 0.02 and could be as low as 0.006% when σ equaled to 0.16. For the data segments that were shorter than 1-min long, the MAPEs of MNF and MDF increased especially for the small values of σ. As shown in Fig. 9, the errors computed over the ECG data length of 10 s increase to 40.14% and 41.64% respectively for the MNF and MDF with the σ value of 0.01. It is clear from the results of simulation studies that the estimation accuracy of the frequency parameters MNF and MDF calculated over the ECG data length less than 30 s are sensitive to not only the data length but also the values of σ, and that the MAPEs calculated over the ECG data length of 1 min are less than 5% for the range of σ from 0.02 to 0.05. This range of such ultra-short-term HRV σ of RRIs is estimated from the clinical ECG recordings in PTBDB. Hence, it is reasonable to use the data of 1-min length for the PDS analysis and its frequency parameter estimation.

Furthermore, the values of HRV, MNF and MDF calculated on each randomly extracted segment of 10 s, 30 s, 1 min, 5 mins, 10 mins, 20 mins, 30 mins, 40 mins, 50 mins and 60 mins from 33 clinical ECG signals with ST-segment elevation in EDB were presented in Figs. 10. It can be seen from Fig. 10(a) that the HRV trended to increase with longer data lengths, which is consistent with the early study that demonstrated the longer recordings are associated with increased HRV [7], [35], [40]. The statistical results showed that all the ultra-short-term HRVs (10 s, 30 s, 1 min) had significant differences compared with those calculated from 60-min data ($p < 0.0001$). From Figs. 10(b) and 10(c), it can be observed that the Mean $\pm$ SD of MNF and MDF of 1 min data were 6.64 ± 1.80 Hz and 4.54 ± 2.20 Hz respectively, which were close with those of 60 mins (6.60 ± 1.81 Hz and 4.50 ± 2.16 Hz). The statistical results showed that there were no significant differences between MNF and MDF of 1 min and those of 60 mins ($p = 0.36$; $p = 0.37$). The MNF and MDF were relatively stable over the entire data lengths tested and showed no statistically significant differences in comparison with those calculated from the 60-min segments except for the segment
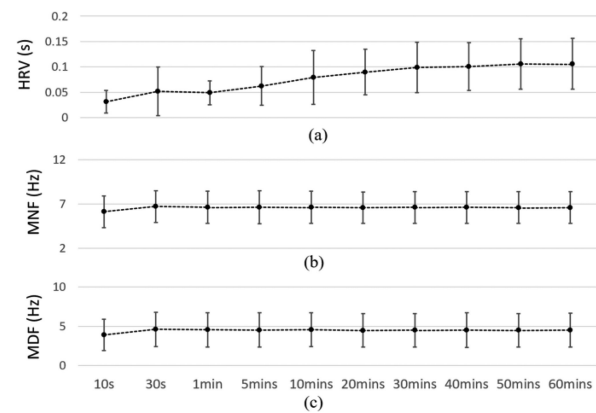

Fig. 10. The values of (a) HRV, (b) MNF and (c) MDF over different ECG lengths from 33 STEMI patients. The values are expressed as Mean $\pm$ SD.

length of 10 s. The results from the clinical ECGs indicated that although the length of the ECG recording will affect the HRV estimation, the MNF and MDF were nearly constant over the entire range of data lengths except for the segment of 10 s. All the results of simulation and clinical studies strongly suggested that the MNF and MDF calculated from ultra-short-term ECGs could be potential indicators of STEMI.

According to the previous reports and guidelines, the data length for HRV analysis range from less than 1 min to over 24 h, which are classified into long-term recordings (≥ 24 h), short-term recordings (2~5 min) and ultra-short-term recordings (<2 min) [7], [8], [35]. Long-term and short-term analyses reflect different underlying physiological meanings and cannot substitute for each other [8], [35]. Long-term HRV may be attribute to fluctuations in circadian rhythms, core body temperature, metabolism, the sleep cycle, and the renin–angiotensin system while the short-term HRVs are associated with four interdependent sources: (1) the complex interaction between the sympathetic and parasympathetic activities; (2) respiratory sinus arrhythmia; (3) the baroreceptor reflex that regulates the fast responses to changes in blood pressure; and (4) rhythmic adjustments in blood vessel diameter [8], [34]. However, the

short-term HRV metrics has not been integrated in routine clinical practice partially because of its high assessment time cost. The short-term HRV measurement of 5 mins is prohibitively long when compared with other physiological parameters commonly used clinically and in home environments such as blood pressure, heart rate, core body temperature, breath rate, oxygen saturation, blood glucose, and body weigh [41]. Hence, some research efforts have been spent on investigating the validity of ultra-short-term HRV as a surrogate of short-term HRV in recent years especially for the SDNN which is the HRV parameter used in this study. Several studies concluded that the ultra-short-term HRV calculated from the ECG recording of 60 s can surrogate short-term HRV in mental stress investigation, sport research area and diabetes mellitus patients [9], [42], [43], [44]. One study even recommended either 30 s or multiple 10 s ECG recordings for ultra-short-term HRV calculation based on a large sample size of 3387 subjects [45]. Additionally, due to the development of wearable sensors in the healthcare and consumer devices, the demands of ultra-short-term HRV analysis using less than 5-min data for monitoring individual's health status is increasing [46]. Many mobile applications and wearable devices are being released into the market, claiming to measure HRV in real time (from 10 s to 1 min) [10].

In summary, the simulation results showed that MNF presented a linear relationship with HRs for given HRVs, and the changes in MNF were within small changes in the values of λ and σ in the tested physiological range. Although MDF was nonlinear with PPT statistics and exhibited slightly larger fluctuations compared with MNF for the same range of λ and σ, the shift ratios of MDF (51.39 ± 12.94%, 47.41 ± 10.80%, 50.72 ± 15.56%) were higher than MNF (38.27 ± 11.64%, 37.86 ± 10.83%, 36.06 ± 14.93%) in three types of STEMI, which indicated that the MDF was more sensitive to the alterations in P-QSR-T complexes than the MNF. Strictly speaking, the values of MNF and MDF depended on both PPT statistics and the waveform of P-QSR-T complexes, reflecting the effects of nervous control and heart contraction dynamics. However, the changes in MNF and MDF caused by λ and σ in ECG of 60 s were relatively small, and instead they were dominated by morphological changes in P-QSR-T complexes.

In addition to the interactive effects of PPT statistics on MNF and MDF studied in ultra-short-term ECG of 60 s, MNF and MDF over different ECG lengths from 10 s to 60 mins were further tested on clinical ECG signals of longer segment lengths from 33 patients with STEMI diseases in EDB. The frequency parameters calculated from the ECG data longer than 10 s consistently showed no significant differences compared with those calculated from 60 mins. With further tests on a larger database, the MNF, MDF and frequency shift ratios of ultra-short-term ECG could become new indicators for the screening and diagnosis of STEMI diseases.

IV. CONCLUSION

A mathematical model of ECG signal has been proposed for studying the interactive effects of heart pacing statistics and heart contraction related P-QRS-T complexes on the ECG power spectrum with attempt to its application for the diagnosis of STEMI diseases. The following conclusions can be drawn from the results of theoretical analysis supported by experimental and simulation studies: 1) main peaks in the PDS of ECG signal are normally introduced at the pacing/heart rate and its harmonics as shown in Figs. 2, 3, 4 and 8; 2) the magnitudes and numbers of the PDS peaks depend on the normalized HRV, c and further, the lower the HRV, the larger the magnitudes of peaks along with the increasing number of distinct PDS peaks as seen in Figs. 2, 3; and 3) the overall envelope of the PDS of ECG signal is determined by the spectrum of the P-QRS-T complexes while the detailed changes are associated with the RRIs statistics as illustrated in Figs. 4 and 8; and 4) it is further observed in experimental PDS data analysis and model simulation that there is a distinct and consistent frequency shift towards the lower frequency range in the PDSs of ST-elevated ECG leads in comparison with those reference leads on the same STEMI patients. Furthermore, based on the clinical analysis, it was found that the MNF, MDF and their frequency shift ratios displayed clear differences between STEMI patients and healthy subjects. It has been demonstrated through the tests on simulated and clinical longer ECG signals with ST-segment elevation that with the minimal effects of HR and HRV, the proposed frequency parameters obtained from ultra-short-term ECG of 60 s (or even shorter to 30 s) can differentiate the STEMI patients from healthy subjects with the same level of accuracy achieved by the frequency parameters over longer ECG signals of 60 mins, which provided the possibility of using the ultra-short-term frequency parameters in wearable devices to qualitatively measure the frequency shift phenomena for the diagnosis of STEMI diseases in living-free environments.

However, it is worth emphasizing that the ECG spectral analysis is an evolving technology and that the future will undoubtedly see major advances especially with the ever-increasing development in ultra-short-term analysis and its applications in wearable based-mHealth for the preventive medicine. We envision that these advances to improve the technology and its applications will be in three general areas. First, mathematical model improvement in taking into account the nonlinearity and non-stationary dynamics in HRV and the beat-to-beat variations in the morphology of P-QRS-T complexes [47], [48], [49] are possible. Second, innovations in control of artifacts and false heartbeats through the novel designs of wearable recording devices and signal processing algorithms will lead to improvement in ECG spectral parameter estimation accuracy. Third, further studies search compelling evidence that these ultra-short-term metrics in the frequency domain can forecast real-world health or performance outcomes based on a large clinical ECG data base. Moreover, with continuing advances in ECG frequency domain research, as reflected in this paper, it is also believed that the applications of the spectral modeling approaches can move beyond the diagnosis of STEMI to the studies of other cardiovascular diseases such as pericarditis and to the monitoring of the health and emotion statuses [50] of pilot, driver and other individuals. Further efforts to conduct model-based spectral analysis that has direct and practical implications with clinical applications will be of utmost importance.

With these advances, we foresee the ultra-short-term ECG metrics in the frequency domain such as the MNF, MDF and the frequency shift ratio of MNF and MDF will become a powerful tool for the detection, diagnosis, monitoring, management, and study of CVDs, but it will not replace the time domain methods currently used in clinical practice.

APPENDIX I

The probability density function of the Gaussian distributed random R-R intervals, x, can be described as:

$$f_x\ (x) = \frac{1}{\sqrt{2\pi}\sigma_x}\ e^{\frac{-(x-\frac{1}{\lambda})^2}{2\sigma_x^2}}, \tag{A1}$$

where $\frac{1}{\lambda}$, is the mean and σ_x, the HRV, is the standard deviation of the RRI distribution. The Fourier transform of the $f_x(x)$ becomes,

$$F_x\ (f) = e^{-\frac{i2\pi f}{\lambda}}\ e^{-2(\pi\sigma_x f)^2}. \tag{A2}$$

According to the Euler's formula, F_x and F_x^* can be described respectively as,

$$F_x\ (f) = e^{-2(\pi\sigma_x f)^2}\ [cos\,(2\pi f/\lambda) - isin\,(2\pi f/\lambda)], \tag{A3}$$

and

$$F_x^*\ (f) = e^{-2(\pi\sigma_x f)^2}\ [cos\,(2\pi f/\lambda) + isin\,(2\pi f/\lambda)]. \tag{A4}$$

Substituting (A3) and (A4) to (4) yields,

$$\Phi_{pp} = \lambda\frac{2\left(\frac{e^{2(\pi\sigma_x f)^2}-e^{-2(\pi\sigma_x f)^2}}{2}\right)}{2\left[\frac{e^{2(\pi\sigma_x f)^2}+e^{-2(\pi\sigma_x f)^2}}{2} - cos\,(2\pi f/\lambda)\right]} \tag{A5}$$

Owing to,

$$\frac{e^{2(\pi\sigma_x f)^2} - e^{-2(\pi\sigma_x f)^2}}{2} = \sinh\left[2(\pi f\sigma_x)^2\right] \tag{A6}$$

and

$$\frac{e^{2(\pi\sigma_x f)^2} + e^{-2(\pi\sigma_x f)^2}}{2} = \cosh\left[2(\pi f\sigma_x)^2\right], \tag{A7}$$

we can get,

$$\Phi_{pp} = \lambda\frac{sinh\left[2(\pi f\sigma_x)^2\right]}{\cosh\left[2(\pi f\sigma_x)^2\right] - cos\,(2\pi f/\lambda)}. \tag{A8}$$

Substituting (A8) into (3) yields finally (6).

REFERENCES

[1] A. C. Guyton and J. E. Hall, *Text Book of Medical Physiology*. 8th ed., Philadelphia, PA, USA: VVB Saunders, 1991, pp. 159–169.

[2] S. J. Morgan and J. A. M. Mora, "Effect of heart rate variability biofeedback on sport performance, a systematic review," *Appl. Psychophysiol. Biofeedback*, vol. 42, no. 3, pp. 235–245, 2017.

[3] B. Xhyheri et al., "Heart rate variability today," *Prog. Cardiovasc. Dis.*, vol. 55, no. 3, pp. 321–331, 2012.

[4] U. R. Acharya et al., "Heart rate variability: A review," *Med. Biol. Eng. Comput.*, vol. 44, no. 12, pp. 1031–1051, 2006.

[5] E. Buccelletti et al., "Heart rate variability and myocardial infarction: Systematic literature review and metanalysis," *Eur. Rev. Med. Pharmacol. Sci.*, vol. 13, no. 4, pp. 299–307, 2009.

[6] V. H. Huikuri and P. K. Stein, "Heart rate variability in risk stratification of cardiac patients," *Prog. Cardiovasc. Dis.*, vol. 56, no. 2, pp. 153–159, 2013.

[7] Electrophysiology, Task Force of the European Society of Cardiology the North American Society of Pacing, "Heart rate variability: Standards of measurement, physiological interpretation, and clinical use," *Circulation*, vol. 93, no. 5, pp. 1043–1065, 1996.

[8] F. Shaffer, M. Z. Meehan, and C. L. Zerr, "A critical review of ultra-short-term heart rate variability norms research," *Front. Neurosci.*, vol. 14, 2020, Art. no. 594880.

[9] L. Salahuddin, J. Cho, M. G. Jeong, and D. Kim, "Ultra short term analysis of heart rate variability for monitoring mental stress in mobile settings," in *Proc. 29th Annu. Int. Conf. IEEE Eng. Med. Biol. Soc.*, 2007, pp. 4656–4659.

[10] L. Pecchia et al., "Are ultra-short heart rate variability features good surrogates of short-term ones? State-of-the-art review and recommendations," *Healthcare Technol. Lett.*, vol. 5, no. 3, pp. 94–100, 2018.

[11] F. Lombardi, "Chaos theory, heart rate variability, and arrhythmic mortality," *Circulation*, vol. 101, no. 1, pp. 8–10, 2000.

[12] A. Voss et al., "Methods derived from nonlinear dynamics for analysing heart rate variability," *Philos. Trans. Roy. Soc. A: Math., Phys. Eng. Sci.*, vol. 367, no. 1887, pp. 277–296, 2009.

[13] V. L. Roger, "Epidemiology of myocardial infarction," *Med. Clin. North Amer.*, vol. 91, no. 4, pp. 537–552, 2007.

[14] B. Ibanez et al., "2017 ESC guidelines for the management of acute myocardial infarction in patients presenting with ST-segment elevation: The task force for the management of acute myocardial infarction in patients presenting with ST-segment elevation of the European Society of Cardiology (ESC)," *Eur. Heart J.,* vol. 76, no. 2, pp. 229–313, 2018.

[15] U. R. Acharya et al., "Automated detection and localization of myocardial infarction using electrocardiogram: A comparative study of different leads," *Knowl.-Based Syst.*, vol. 99, pp. 146–156, 2016.

[16] A. B. de Luna, M. Fiol-Sala, and E. M. Antman, "The 12 lead ECG in ST elevation myocardial infarction," in *A Practical Approach for Clinicians*. Hoboken, NJ, USA: Wiley, 2008.

[17] E. Tragardh et al., "Detection of acute myocardial infarction using the 12-lead ECG plus inverted leads versus the 16-lead ECG (with additional posterior and right-sided chest electrodes)," *Clin. Physiol. Funct. Imag.*, vol. 27, no. 6, pp. 368–374, 2010.

[18] M. Sharma, R. S. Tan, and U. R. Acharya, "A novel automated diagnostic system for classification of myocardial infarction ECG signals using an optimal biorthogonal filter bank," *Comput. Biol. Med.*, vol. 102, pp. 341–356, 2018.

[19] A. L. A. Blanco et al., "ECG sonification to support the diagnosis and monitoring of myocardial infarction," *J. Multimodal User Interfaces.*, vol. 14, pp. 207–218, 2020.

[20] R. K. Tripathy, A. Bhattacharyya, and R. B. Pachori, "A novel approach for detection of myocardial infarction from ECG signals of multiple electrodes," *IEEE Sens. J.,* vol. 19, no. 12, pp. 4509–4517, 2019.

[21] J. Zhang et al., "Automated detection and localization of myocardial infarction with staked sparse autoencoder and treebagger," *IEEE Access*, vol. 7, pp. 70634–70642, 2019.

[22] Y. Kotriwar et al., "Higher order spectral analysis of ECG signals," in *Proc. Biomed. Signal Process. Control*, 2018, pp. 1–8.

[23] G. B. Stanley, K. Poolla, and R. A. Siegel, "Threshold modeling of autonomic control of heart rate variability," *IEEE Trans. Biomed. Eng.*, vol. 47, no. 9, pp. 1147–1153, Sep. 2000.

[24] R. D. Berger, S. Akselrod, D. Gordon, and R. J. Cohen, "An efficient algorithm for spectral analysis of heart rate variability," *IEEE Trans. Biomed. Eng.*, vol. BME-33, no. 9, pp. 900–904, Sep. 1986.

[25] R. Barbieri et al., "A point-process model of human heartbeat intervals: New definitions of heart rate and heart rate variability," *Amer. J. Physiol.-Heart Circulatory Physiol.*, vol. 288, no. 1, pp. H424–H435, 2005.

[26] J. H. Cha and M. Finkelstein, "Point processes for reliability analysis renewal processes and applications," in *Springer Series in Reliability Engineering.* Berlin, Germany: Springer, ch. 3, 2018, pp. 37–71.

[27] Y. T. Zhang et al., "Distributed random electrical neuromuscular stimulation: Effects of the inter-stimulus interval statistics on the EMG spectrum and frequency parameters," *J. Rehabil. Res. Develop.*, vol. 31, no. 4, 1994, Art. no. 303.

[28] Z. S. Pan, Y. Zhang, and P. A. Parker, "Motor unit power spectrum and firing rate," *Med. Biol. Eng. Comput.*, vol. 27, no.no. 1, pp. 14–18, 1989.

[29] G. D. Clifford et al., "Model-based filtering, compression and classification of the ECG," *Int. J. Bioelectromagnetism*, vol. 7, no. 1, pp. 158–161, 2005.

[30] D. R. Cox and W. L. Smith, "On the superposition of renewal processes," *Biometrika*, vol. 41, no. 1/2, pp. 91–99, 1954.

[31] D. R. Cox, *The Statistical Analysis of Series of Events*. London, U.K.: Methuen & Co., 1966.

[32] B. Lindner, "A brief introduction to some simple stochastic processes," in *Stochastic Methods Neuroscience*, vol. 1. Oxford, U.K.: Oxford Univ. Press, 2009.

[33] W. Gerstner *et al.*, "Neuronal dynamics: From single neurons to networks and models of cognition," Cambridge, U.K.: Cambridge Univ. Press, 2014.

[34] P. PhysioBank, "PhysioNet: Components of a new research resource for complex physiologic signals," *Circulation.*, vol. 101, no. i23, pp. e215–e220, 2000.

[35] F. Shaffer and J. P. Ginsberg, "An overview of heart rate variability metrics and norms," *Front. Public Health*, vol. 5, 2017, Art. no. 258.

[36] D. Öztuna *et al.*, "Investigation of four different normality tests in terms of type 1 error rate and power under different distributions," *Turkish J. Med. Sci.,* vol. 36, no. 3, pp. 171–176, 2006.

[37] A. K. Bhoi *et al.*, "A significant approach to detect heart rate in ECG signal," *Int. J. Adv. Elect. Electron. Eng. (IJAEEE)*, vol. 1, no. 1, 2012.

[38] M. A. Quiroz-Juárez *et al.*, "Generation of ECG signals from a reaction-diffusion model spatially discretized," *Sci. Rep.*, vol. 9, Dec. 2019, Art. no. 19000.

[39] H. Weisberg and H. F. Weisberg, *Central Tendency and Variability*, Thousand Oaks, CA, USA: Sage, 1992, no. 83.

[40] J. P. Saul *et al.*, "Analysis of long term heart rate variability: Methods, 1/f scaling and implications," *Comput. Cardiol.*, vol. 14, pp. 419–422, 1988.

[41] F. Shaffer *et al.*, "The promise of ultra-short-term (UST) heart rate variability measurements: A comparison of pearson product-moment correlation coefficient and limits of agreement (LoA) concurrent validity criteria," in *Physiological Recording Technology and Applications in Biofeedback and Neurofeedback*, D. Moss and F. Shaffer, Oakbrook Terrace, Eds. IL, USA: Association for Applied Psychophysiology and Biofeedback, 2019, pp. 214–220.

[42] R. Castaldo *et al.*, "Ultra-short term HRV features as surrogates of short term HRV: A case study on mental stress detection in real life," *BMC Med. Informat. Decis. Mak.*, vol. 19, no. 1, pp. 1–13, 2019.

[43] U. Nussinovitch *et al.*, "Evaluating reliability of ultra-short ECG indices of heart rate variability in diabetes mellitus patients," *J. Diabetes Complications,* vol. 26, no. 5, pp. 450–453, 2012.

[44] M. R. Esco *et al.*, "Ultra-shortened time-domain HRV parameters at rest and following exercise in athletes: An alternative to frequency computation of sympathovagal balance," *Eur. J. Appl. Physiol.*, vol. 118, no. 1, pp. 175–184, 2018.

[45] M. L. Munoz *et al.*, "Validity of (ultra-) short recordings for heart rate variability measurements," *PloS One*, vol. 10, no. 9, 2015, Art. no. e0138921.

[46] R. Castaldo *et al.*, "Ultra-short term HRV features as surrogates of short term HRV: A case study on mental stress detection in real life," *BMC Med. Inform. Decis. Mak.*, vol. 19, no. 1, pp. 1–13, 2019.

[47] Z. Chen, E. N. Brown, and R. Barbieri, "Characterizing nonlinear heartbeat dynamics within a point process framework," *IEEE Trans. Biomed. Eng.*, vol. 57, no. 6, pp. 1335–1347, Jun. 2010.

[48] P. E. McSharry, G. D. Clifford, L. Tarassenko, and L. A. Smith, "A dynamical model for generating synthetic electrocardiogram signals," *IEEE Trans. Biomed. Eng.*, vol. 50, no. 3, pp. 289–294, Mar. 2003.

[49] M. A. Quiroz-Juarez *et al.*, "Quasiperiodicity route to chaos in cardiac conduction model," *Commun. Nonlinear Sci. Numer. Simul.*, vol. 42, pp. 370–378, Jan. 2017.

[50] A. Rozanski *et al.*, "Association of optimism with cardiovascular events and all-cause mortality: A systematic review and meta-analysis," *JAMA Netw. Open*, vol. 2, no. 9, 2019, Art. no. 1912200.